energies

MDPI

Article

Dynamic Cascading Simulations of Hybrid AC/DC Power Systems in PSS/E

Saeed Rezaeian-Marjani *, Lukas Sigrist and Aurelio García-Cerrada

Instituto de Investigación Tecnológica (IIT), ETSI ICAI, Universidad Pontificia Comillas, 28008 Madrid, Spain; lsigrist@comillas.edu (L.S.); aurelio@comillas.edu (A.G.-C.)

* Correspondence: srezaeian@comillas.edu; Tel.: +34-91542-2800 (ext. 4523)

Abstract

Power system blackouts remain a major concern for modern electricity networks, as they often result from cascading failures that lead to substantial load shedding and widespread service disruptions. This paper presents a dynamic resilience assessment of hybrid AC/DC power systems and investigates the effectiveness of voltage-source-converter-based high-voltage direct current (VSC-HVDC) technology in enhancing system resilience under outage contingencies. The study contributes by integrating protection devices and their settings into the analysis and by providing a quantitative evaluation of the system response to N-2 and N-3 contingencies using PSS®E simulations. The demand not served index is used as a measure of resilience, and its cumulative distribution functions are computed to compare the performance of AC and DC interconnections. The results underscore the importance of VSC-HVDC links in mitigating cascading failures, highlighting their potential as a resilience-enhancing component in modern power grids.

Keywords: resilience; dynamic simulation; contingency analysis; VSC-HVDC

1. Introduction

The expansion of interconnected power grids enhances power transfer efficiency, but increases the risk of large-scale blackouts from cascading failures [1].

Preventing cascading failures is crucial for enhancing system resilience, as it helps limit the extent, severity, and duration of system degradation following an extreme event [2]. In complex power systems, cascading effects can amplify initial disturbances, potentially leading to widespread blackouts and significant socio-economic impacts. By mitigating these risks, operators can facilitate a faster recovery, maintain critical services, and reduce the grid's overall vulnerability. Resilient system design should include advanced monitoring, protection, and control strategies that effectively address the threat of cascading failures [3].

As highlighted in [4], intelligent energy management and advanced control strategies can ensure smooth and uninterrupted operation of grids. Voltage-source-converter-based high-voltage direct current (VSC-HVDC) technology offers significant benefits for long-distance power transmission, asynchronous network interconnection, and underground and undersea connections, including the integration of offshore renewable energy resources. Thanks to their inherent controllability, VSC-HVDC systems can enhance the resilience, security, and stability of hybrid AC/DC power systems. In addition to these capabilities, VSC-HVDC can further reduce the risk of cascading failures by enhancing grid controllability and stability. It serves as an electrical firewall to limit the propagation of disturbances between network areas [5].

Received: 6 February 2026
Revised: 27 February 2026
Accepted: 10 March 2026
Published: 25 March 2026

Previous studies have made valuable contributions to power system operation and control, particularly in the context of VSC-HVDC systems, by examining expected contingencies under steady-state conditions. For instance, in [6], VSC-HVDC integration was shown to enhance steady-state performance and effectively manage N-1 contingencies by reducing losses and mitigating voltage violations. A contingency analysis method for integrated AC/DC grids was proposed in [7], highlighting the role of VSC-HVDC in power-flow control and overload mitigation under steady-state and contingency conditions. In [8], the role of HVDC controllability in reducing preventive and curative redispatch under contingency scenarios was analyzed using security-constrained optimal power flow in a mixed AC/DC grid.

While these static approaches provide computational efficiency and valuable insights into post-contingency behavior, they are limited in their ability to capture dynamic responses and evaluate system stability, protection mechanisms, and disturbance propagation. In this context, several studies have examined the dynamic responses of power systems utilizing VSC-HVDC links under expected contingencies. In [9], a linearized real-time contingency analysis method was proposed for AC/DC grids with multiple VSC-HVDC stations. The method combines steady-state sensitivity analysis with validation through dynamic EMT simulations in Simulink using the SimPowerSystems package. This hybrid approach ensures both computational efficiency and dynamic accuracy. In [10], a time-domain-based local fault identification method that utilizes real-time measurements at VSC-HVDC substations was proposed, focusing on dynamic behavior and pattern recognition during faulted operation. Simulation results obtained using DIgSILENT PowerFactory were provided. In [11], dynamic contingency scenarios involving VSC-HVDC retrofitting in the Italian grid were analyzed and simulated in DIgSILENT PowerFactory. The study confirmed that VSC-based control significantly mitigates frequency and voltage fluctuations, reducing recovery time and improving system resilience against local faults. In [12], cascading faults in hybrid AC/DC grids were innovatively analyzed, demonstrating how AC inverter faults can trigger sequential DC and AC line failures. These results were validated through PSCAD/EMTDC simulations. The PSS®E power system simulation software package has been used only sparingly for this purpose.

Although previous studies have primarily focused on system response to single or localized contingencies, they have often neglected detailed protection behavior, relay operations, and network separation. A first step in this direction was taken in [13], which assessed the impact of HVDC links on the demand not served (DNS) in resilience studies, considering overcurrent, underfrequency, overfrequency, and undervoltage relays. However, although ref. [13] included various protection mechanisms, it did not systematically analyze the influence of relay parameter settings on the propagation of cascading failures, nor did it investigate the sensitivity of dynamically computed DNS to protection coordination.

In [14], it was shown that proper coordination between protection systems and VSC-HVDC links could mitigate cascading failures. While the study highlighted the effectiveness of coordinated control in reducing line currents and maintaining voltage stability, it did not explicitly quantify resilience using a dynamic DNS metric or examine its time-domain evolution during cascading disturbances.

An integrated control and DC protection strategy was proposed in [15] to economically compensate for power losses caused by HVDC line outages without load shedding or reducing transmitted power. Nevertheless, its focus was primarily on coordinated control for specific HVDC outages rather than on large-scale propagation of cascading failures under severe N-k contingencies with detailed protection parameter settings.

In contrast to previous studies, this paper advances the state of the art in three key directions. First, unlike static cascading analyses [6–8] that assess only steady-state post-

contingency conditions, this work employs dynamic time-domain simulations to capture the temporal evolution of cascading failures. Second, while EMT-based studies [9,12] provide high transient accuracy, they are computationally intensive for large-scale cascading analysis; the PSS®E-based RMS simulations employed in this study offer a scalable alternative that balances fidelity with computational feasibility. Third, building on prior DNS-based assessments [13,14] that incorporate basic protection models, this paper systematically evaluates the sensitivity of protection relay parameters and quantifies resilience through a dynamically computed DNS index under severe N-k contingencies. Although this study also analyzes N-1 contingencies, the results presented focus on N-2 and N-3 contingency scenarios. N-1 contingencies represent the simplest and most common single-element failures that power systems are typically designed to withstand. In contrast, N-2 and N-3 contingencies represent more severe and less probable system disturbances and are critical for assessing the network's robustness and resilience under extreme conditions. The main contributions of this paper are summarized as follows:

- Comprehensive modeling of protection devices and evaluation of the impact of their settings on cascading outage propagation, an aspect largely neglected in previous studies.
- Quantification of cascading outage severity through a dynamically computed DNS index within a time-domain simulation framework, instead of traditional static methods, enabling a more accurate and realistic representation of protection actions, system dynamics, and cascading effects.
- Investigation of the mitigation capability of VSC-HVDC links in limiting disturbance propagation and enhancing system resilience.
- Implementation of a fully automated PSS®E-based simulation tool, ensuring that the proposed methodology and results are directly applicable to real-world power system operation and planning.

The paper is structured as follows: Section 2 outlines the methodology. Section 3 describes the dynamic modeling of VSC-HVDC, including VSC control and the representation of the DC grid. Section 4 addresses the modeling of protection devices, including overcurrent relays, underfrequency load shedding, and generator protection. Section 5 introduces the test system, while Section 6 presents simulation results for N-2 and N-3 contingencies, as well as DNS sensitivity to the relay settings. Finally, Section 7 concludes the paper.

2. Methodology

The methodology presented in this study allows for a systematic evaluation of the dynamic response and cascading behavior of hybrid AC/DC power systems under various contingency scenarios. This includes HVDC links integrated into AC systems and interconnections between asynchronous AC networks. The simulation framework combines PSS®E 34.9.6 (Siemens Power Technologies International (PTI), Schenectady, NY, USA), a professional power system simulation tool, with Python 2.7.18-based automation to efficiently generate, execute, and post-process scenarios. The overall methodology is depicted in

This flowchart illustrates that three distinct categories of inputs are essential for the simulation: the initial static model, the dynamic model, and the triggering event. The triggering event may be generated by a specialized event simulator or defined hypothetically using an Excel-based event file. This event is then provided to the program to initiate the simulation. Based on the triggering event, the simulation determines whether cascading outages occur and whether the power system can withstand them. Figure 1.

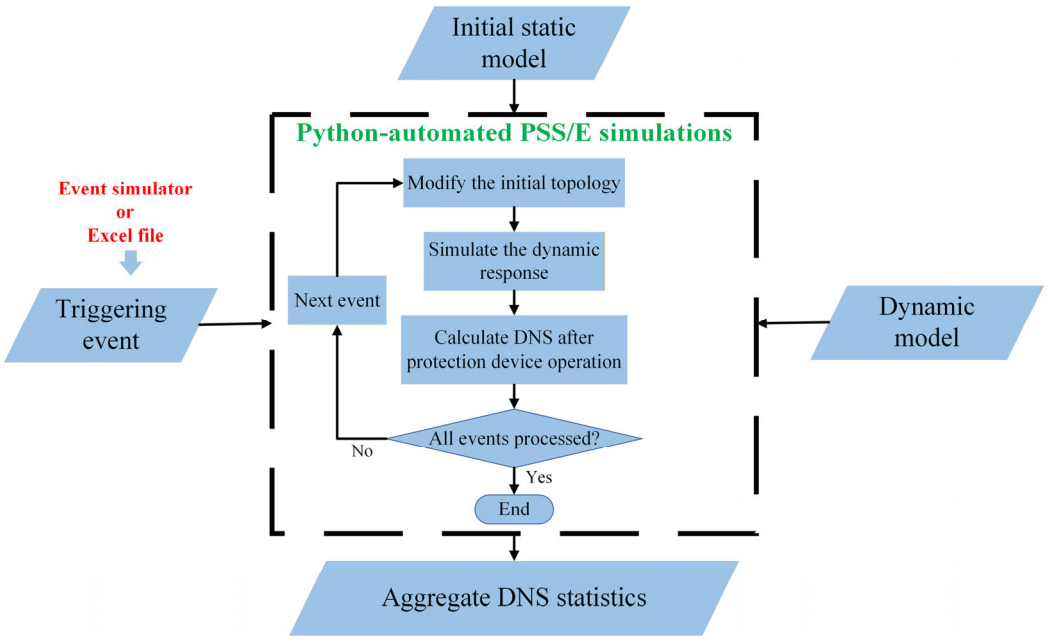

Figure 1. Flowchart of the simulation process for assessing cascading propagation and load shedding in AC/DC linked grids.

The core of the proposed methodology is implemented through automated simulations in PSS®E 34.9.6 using Python 2.7.18, which serves as the engine for executing cascading contingency scenarios. Before applying the triggering events, a steady-state power flow is solved to initialize the subsequent dynamic simulation properly. After each triggering event, the network topology is updated. While the dynamic models and parameters remain unchanged, the status of system components is updated to reflect the post-contingency operating state. If a power system component trips during the simulation due to the action of protection devices, its current injection is set to zero, and the network topology is updated.

Protective devices are designed to respond to abnormal conditions in an electrical system. When activated, they can cause components to disconnect or reconfigure the system. The actions taken by these devices directly affect the amount of load curtailment, which is measured after each simulation.

To quantitatively assess system resilience, load curtailment is evaluated using the DNS index, a widely used metric that quantifies the amount of demand not served during outages [16]. A lower DNS indicates that the system is better able to maintain supply under disturbances, while a higher DNS highlights the system's vulnerabilities and the extent of service interruptions. This index is calculated based on the difference between the expected demand and the load actually served at the end of the simulation. For contingency c, DNS is defined in (1).

$$DNS_c = \sum_{i=1}^{N} \left(\underbrace{P_i^{demand} - P_i^{served}}_{P_i^{shed}} \right) \quad (1)$$

where N denotes the total number of load buses in the system, P_i^{demand} denotes the expected demand at load bus i, P_i^{served} denotes the load actually served at load bus i in the final simulation state, and P_i^{shed} denotes the load shedding (or demand not served) at load bus i. It should be noted that in this paper, DNS is reported as the final instantaneous unserved load (MW), computed as the difference between the total pre-contingency demand and the served load at the end of the simulation horizon. Voltage and frequency behavior

are represented in the time-domain simulations via dynamic and protection models, and the effects are reflected in DNS. Nonetheless, explicit voltage/frequency indices are not considered and are outside the scope of this work.

This iterative process is carried out for all considered contingencies to assess system robustness under various operating and contingency conditions. The analysis also considers the type of interconnection and its ability to contain disturbances.

The simulations aim to compare the effectiveness of AC and DC interconnections in mitigating cascading effects. In particular, the study assesses whether DC links can isolate disturbances and limit their propagation more effectively than conventional AC interconnections.

Given that this paper focuses on resilience, particular attention is paid to the upper tail of the frequency distribution constructed from the DNS values obtained across the considered contingencies, since it reflects low-probability, high-impact events. To quantify this tail behavior, Conditional Value at Risk (CVaR) is employed as a single risk metric. At confidence level α, CVaR is defined as the expected DNS conditioned on being greater than or equal to the corresponding Value at Risk (VaR):

$$CVaR_{\alpha}(DNS) = \mathrm{E}[DNS | DNS \geq VaR_{\alpha}(DNS)] \tag{2}$$

where $VaR_{\alpha}(DNS)$ is the α-quantile of this distribution, i.e., the smallest threshold γ such that at least a fraction α of DNS values are less than or equal to it. It is obtained as follows [17]:

$$VaR_{\alpha}(DNS) = min\{\gamma | \mathrm{P}(DNS \leq \gamma) \geq \alpha\} \tag{3}$$

where $\mathrm{P}(\cdot)$ denotes the probability operator. Also, DNS represents the set of all DNS values obtained for each considered event:

$$DNS = \{DNS_1, DNS_2, \ldots, DNS_{Nc}\} \tag{4}$$

where N_C denotes the total number of considered contingencies.

It is worth noting that the proposed methodology, which integrates protection devices and their settings into the analysis and evaluates system resilience using the DNS index, is not limited to a specific network. Since DNS is a general quantitative measure of curtailed load, and the analysis follows standard simulation practices in PSS®E, the same approach can be applied to different AC/DC hybrid network configurations for resilience assessment under contingencies.

3. Dynamic Modeling of VSC-HVDC

3.1. VSC Modeling and Control Strategy

In this study, the VSC is modeled by using a vector-control approach within a quasi-static framework on the AC side, where the AC voltage is aligned with the d-axis, i.e., $\overline{u}_s = u_s + j0$. Accordingly, the active and reactive power injections at the connection point are expressed as follows:

$$p_s = u_s i_{s,d} \tag{5}$$

$$q_s = -u_s i_{s,q} \tag{6}$$

where $i_{s,d}$ and $i_{s,q}$ are the d- and q-axis components of the current injected by the VSC. The control architecture comprises two hierarchical loops [18]. The inner current control loop, which typically has a time constant in the range of 1–10 ms [19], is modeled as a first-order system relating the current-component setpoints, $i_{s,d}^{ref}$, $i_{s,q}^{ref}$, to the corresponding actual currents (see Figure 2 [20]).

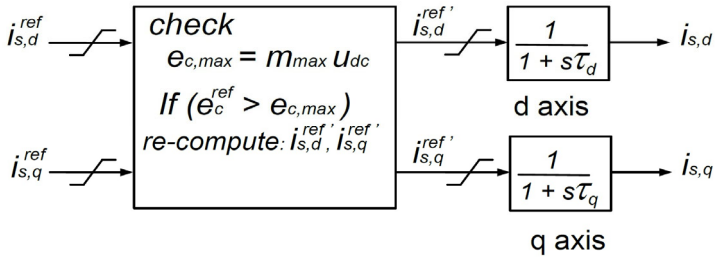

Figure 2. Approximation of the inner current control loop.

With a slower dynamic response (1–100 ms) [19], the outer control loop employs PI controllers to generate the d- and q-axis current references by regulating either the DC voltage or the active power injected into the AC system, and either the reactive power or the AC voltage magnitude, respectively. The outer PI controllers are shown in Figure 3, where $C_x(s)$ represents the transfer function of each controller [20].

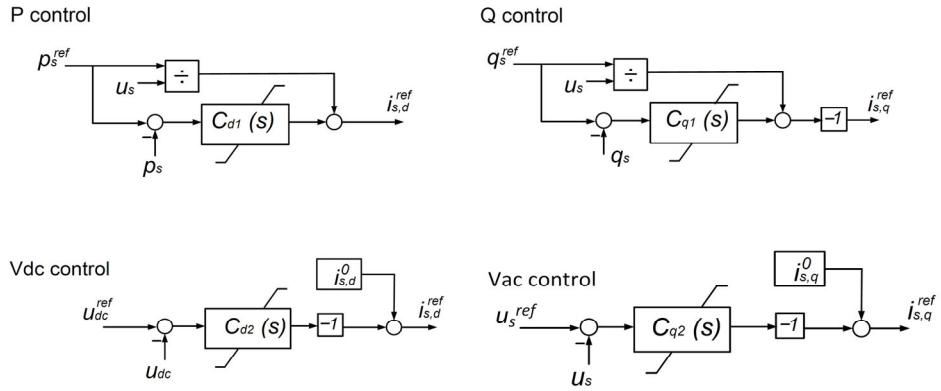

$C_x(s) = K_{p,x} + K_{i,x}/s$ where x can be $d1, d2, q1$ *or* $q2$.

Figure 3. Outer PI controllers.

Operational limits for the converter are enforced within the model, including [21,22]:

- Maximum/minimum active and reactive power limits: P_{max}, P_{min}, Q_{max}, and Q_{min}.
- A current magnitude constraint with configurable prioritization (d-axis, q-axis, or equal).
- A modulation-based constraint on the maximum output AC voltage. If the voltage setpoint exceeds this threshold, the current setpoints are recalculated to remain within the voltage limit.

This control structure enables the VSC to effectively manage power exchange while complying with converter operational constraints, making it suitable for dynamic contingency analysis in AC/DC hybrid systems.

3.2. The Dynamic Model of the DC Grid

The dynamic model of the DC grid comprises converters, capacitors, and cables, as described in [23]. The system inputs are the VSC's current injections. DC cables are represented by an equivalent π-model, with resistance $r_{dc,ij}$, inductance $L_{dc,ij}$ and capacitance $C_{cc,ij}$ as shown in Figure 4.

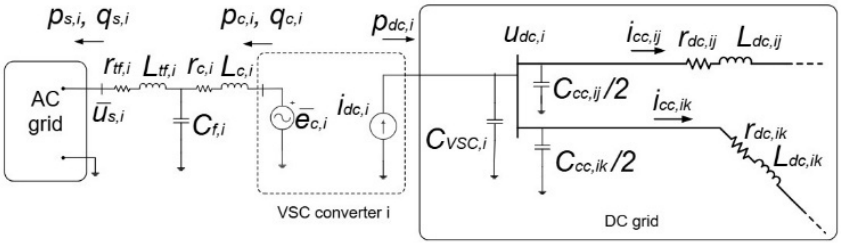

Figure 4. Dynamic model of the DC grid.

An equivalent capacitor is assigned to each DC bus to represent both the converter capacitor, $C_{VSC,i}$, and the capacitance of the connected DC branches, as expressed in (7).

$$C_{dc,i} = C_{VSC,i} + \sum_{i \neq j} \frac{C_{cc,ij}}{2} \tag{7}$$

The model also includes a shunt conductance, $g_{dc,i}$, at each DC bus, which can be used to represent resistive loads. The state variables of the DC system are the DC bus voltages and the DC line currents. Accordingly, the differential equations of the DC grid are given by (8) and (9) [23]:

$$C_{dc} \frac{dU_{dc}}{dt} = -G_{dc} U_{dc} - A_c I_{cc} + I_{dc} \tag{8}$$

$$L_{dc} \frac{dI_{cc}}{dt} = A_c^T U_{dc} - R_{dc} I_{cc} \tag{9}$$

where $U_{dc} = (u_{dc,i}) \in \mathbb{R}^{n \times 1}$ is the vector of DC bus voltages, $I_{cc} = (i_{cc,l}) \in \mathbb{R}^{n_L \times 1}$ is the vector of currents through the DC lines, and $I_{dc} = (i_{dc,i}) \in \mathbb{R}^{n \times 1}$ is the vector of currents injected by the converters into the DC grid. Here, n denotes the total number of DC buses, and n_L denotes the total number of DC lines. Moreover,

$$G_{dc} = diag(g_{dc,i}) \in \mathbb{R}^{n \times n} \tag{10}$$

$$C_{dc} = \text{diag}(C_{dc,i}) \in \mathbb{R}^{n \times n} \tag{11}$$

$$R_{dc} = \text{diag}(r_{dc,l}) \in \mathbb{R}^{n_L \times n_L} \tag{12}$$

$$L_{dc} = \text{diag}(L_{dc,l}) \in \mathbb{R}^{n_L \times n_L} \tag{13}$$

Also, $A_c = (a_{il}) \in \mathbb{R}^{n \times n_L}$ is the incidence matrix of the DC grid, whose elements are defined in (14).

$$a_{il} = \begin{cases} +1 & \text{if line } l \text{ is defined as leaving node } i \\ -1 & \text{if line } l \text{ is defined as entering node } i \\ 0 & \text{if line } l \text{ is not connected to node } i \end{cases} \tag{14}$$

Finally, the AC and DC sides of each converter are coupled through the principle of energy conservation. At each time step, the AC and DC systems are updated sequentially and $p_{dc,i}$ is obtained from $p_{c,i}$. Currents injected into the DC grid are calculated as (15):

$$i_{dc,i} = \frac{p_{dc,i}}{u_{dc,i}} = \frac{-(p_{c,i} + p_{loss,i})}{u_{dc,i}}, \quad \forall i = 1, \ldots, n \tag{15}$$

where $p_{c,i}$ is the active power injected into the AC grid, and $p_{loss,i}$ represents the converter losses, modeled as a quadratic function of the converter AC current, $i_{c,i}$ [24,25]:

$$p_{loss,i} = a_i + b_i . i_{c,i} + c_i . i_{c,i}^2 \tag{16}$$

where a_i, b_i and c_i are converter-specific parameters for each VSC.

4. Protection Devices Modeling in Dynamic Simulation

A wide range of protection devices is utilized in power systems. These devices have a significant impact on the propagation of cascading disturbances. To evaluate the protection system's response under various contingency scenarios, the following types of protective relays were modeled: overcurrent relays, thermal overload relays, underfrequency load shedding relays, and voltage and frequency relays at generator buses. These protection devices have been used in previous studies without further analysis of how their settings affect cascading disturbance propagation [13,26]. In the following, each relay is modeled using mathematical equations consistent with standard protection principles.

4.1. Overcurrent Relay

The time-inverse overcurrent relay operates based on both the magnitude and duration of overcurrent events. It typically comprises two components: an instantaneous unit that trips immediately when the current exceeds a predetermined high threshold, and a time-delayed inverse unit. The operating time of the second unit decreases as the current level increases. The operating time of the inverse unit is defined by (17) [14]:

$$t = \frac{A}{\left(\frac{I}{I_{Pickup}}\right)^k - B} + C \tag{17}$$

where t is the trip time in seconds, I is the current seen by the relay, I_{Pickup} is the pickup current setting of the relay, A, B and C are constants that define the selected time-current characteristic. For the instantaneous unit, the relay trips immediately when $I \geq I_{inst}$, where I_{inst} is the instantaneous pickup current.

4.2. Underfrequency Load Shedding Model

Underfrequency relays disconnect loads when frequency drops significantly due to imbalances between generation and load. The logic-based model activates load shedding when the frequency at bus j, $f_j(t)$, falls below a predefined threshold $f_{th,j,s}$ for a minimum time $t_{d,j,s}$ at shedding stage s [27]. Therefore,

$$z_{j,s}(t) = \begin{cases} 1, & \text{if } f_j(t) < f_{th,j,s} \quad \text{for } \Delta t \geq t_{d,j,s} \\ 0, & otherwise \end{cases} \tag{18}$$

$$P_{shed}^{UFLS}(t) = \sum_{j=1}^{N_b} \sum_{s=1}^{N_{st,j}} P_{j,s}^{nom} . z_{j,s}(t) \tag{19}$$

where $f_j(t)$ is the frequency at bus j at time t, $f_{th,j,s}$ and $t_{d,j,s}$ are the frequency threshold and delay time for the shedding stage s at bus j, $P_{j,s}^{nom}$ is the nominal active load assigned to that stage, and $z_{j,s}(t) \in \{0,1\}$ is the stage trigger signal. Here, N_b denotes the total number of buses equipped with underfrequency load shedding relays, and $N_{st,j}$ is the total number of load-shedding stages at bus j.

4.3. Undervoltage and Overvoltage Protection of Generators

Undervoltage and overvoltage relays are crucial for protecting generators. These relays monitor terminal voltage and trigger a trip if it exceeds or falls below set thresholds for a specific duration, thereby preventing insulation damage or loss of synchronism [28]:

$$Trip_{UV} = \begin{cases} 1, & \text{if } V(t) < V_{min} \text{ for } \Delta t \geq T_{UV} \\ 0, & \text{otherwise} \end{cases} \quad (20)$$

$$Trip_{OV} = \begin{cases} 1, & \text{if } V(t) > V_{max} \text{ for } \Delta t \geq T_{OV} \\ 0, & \text{otherwise} \end{cases} \quad (21)$$

where $V(t)$ is the instantaneous generator terminal voltage, V_{min} and V_{max} are undervoltage and overvoltage thresholds, and T_{UV} and T_{OV} are corresponding delay times.

4.4. Underfrequency and Overfrequency Protection of Generators

Underfrequency and overfrequency relays protect the generator by monitoring the system frequency. The relays trip the generator when the measured frequency remains outside preset limits for a defined time delay [29]. The protection logic is modeled as:

$$Trip_{UF} = \begin{cases} 1, & \text{if } f(t) < f_{min} \text{ for } \Delta t \geq T_{UF} \\ 0, & \text{otherwise} \end{cases} \quad (22)$$

$$Trip_{OF} = \begin{cases} 1, & \text{if } f(t) > f_{max} \text{ for } \Delta t \geq T_{OF} \\ 0, & \text{otherwise} \end{cases} \quad (23)$$

where $f(t)$ is the frequency at the generator terminal, f_{min} and f_{max} are the under- and over-frequency thresholds, and T_{UF} and T_{OF} are the corresponding relay time delays.

5. Description of the Test System

To validate the proposed method in this study, two IEEE 39-bus systems with a nominal voltage of 345 kV are considered. The two systems are connected via an AC or a DC link, representing two separate scenarios. The standard configuration of the IEEE 39-bus test system reported in [30,31] is used, with the following modifications:

- The load demand at all load buses of the primary grid has been reduced by 13%.
- The output power of the power plants in the secondary grid has been reduced by 15%.
- The upper limit of the active power output of the slack generator in the secondary grid was increased from 595 MW to 1000 MW. Consequently, its MVA base was updated from 700 MVA to 1100 MVA.

These modifications were introduced to create a slight imbalance between the two initially identical IEEE 39-bus systems, enabling meaningful power exchange. Without such changes, directly connecting the two networks would result in negligible power flow due to symmetry. This approach ensures realistic interactions between the interconnected networks and provides a valid basis for testing the proposed method.

With the above modifications, the active and reactive power transferred from the primary to the secondary grid are calculated to be 502.9785 MW and −26.8847 MVAr, respectively, confirming that a feasible and stable power flow solution is achieved with all bus voltages and generator outputs within acceptable limits. The AC transmission line is 150 km long and has parameters (resistance, inductance, and charging susceptance) equal to 0.001512 p.u., 0.037807 p.u., and 1.814750 p.u., respectively.

To ensure realistic and stable simulation conditions for the case study, the following main assumptions were considered:

- The AC-side voltages of the VSCs were obtained from the power flow results for the case in which the AC link was present. Accordingly, the AC voltage at the first VSC, connected via a transformer to bus 16 of the primary grid, denoted as $16^{(1)}$, was set to 1.0360 p.u., while the AC voltage at the second VSC, connected via a transformer to bus 4 of the secondary grid, denoted as $4^{(2)}$, was set to 1.0194 p.u.
- The DC-side voltages of the VSCs were set to 400 kV, establishing a nominal operating point for the converters.
- The rated apparent power of the converters was set to 600 MVA, chosen to match the scale of the IEEE 39-bus system and ensure realistic converter operation.
- The transformer reactances between each converter and the corresponding network bus were set to 0.1 p.u. on a 600 MVA base, which was selected to represent voltage drops and current limits reasonably.
- The parameter r_{dc} was set to 2.5 Ω, while L_{dc} and C_{cc} (in Figure 4) were set to 140.085 mH and 1.785 µF, respectively [25].
- The initial DC power transfer was set to 503 MW from the primary to the secondary grid, chosen to match the AC-link power flow and provide a fair basis for comparison between the two scenarios.
- The converter loss model parameters a_i, b_i and c_i are assumed to be 5.25×10^{-3} p.u., 1.65×10^{-3} p.u. and 2.10×10^{-3} p.u., respectively [25].

Table 1 summarizes the controller parameters used for the VSC-HVDC model in this study. These values are obtained from [25] and have been tuned to ensure stable operation under the considered contingency scenarios. The case study is depicted in Figure 5.

Table 1. Outer-loop PI controller parameters of the VSC-HVDC system.

Outer Control Gains	Values
P: prop./int. ($K_{p,d1}/K_{i,d1}$)	0/0
Vdc: prop./int. ($K_{p,d2}/K_{i,d2}$)	2.45 p.u./49 p.u./s
Q: prop./int. ($K_{p,q1}/K_{i,q1}$)	0/0
Vac: prop./int. ($K_{p,q2}/K_{i,q2}$)	10 p.u./100 p.u./s

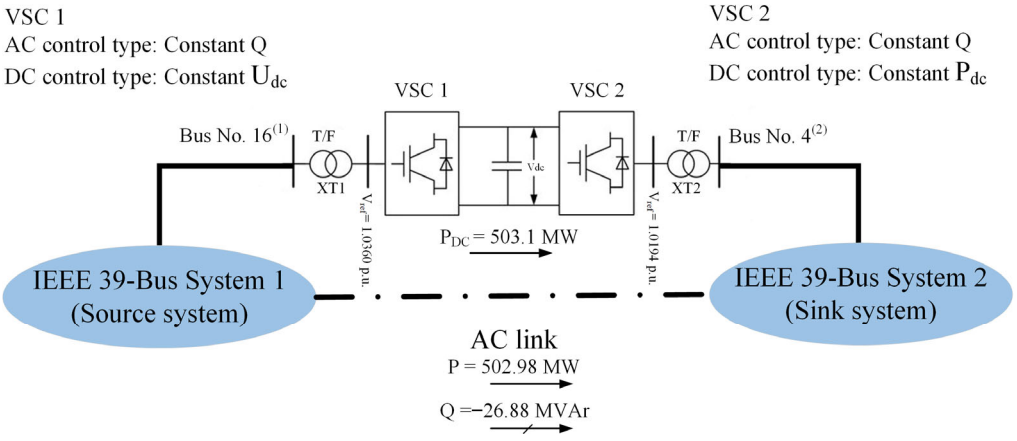

Figure 5. Schematic representation of the case study.

The following assumptions were made regarding the protection equipment implemented in the system:

- **Overcurrent relays:** Each transmission line is equipped with two overcurrent relays, one at the sending end and the other at the receiving end. Transformers are also equipped with overcurrent relays at each terminal. The primary relay is configured

to detect overcurrent conditions based on standard inverse-time characteristics, with threshold (THR) factors set to 1.0 for lines and 1.7 for transformers. The secondary relay detects overload conditions using THR values of 1.05 for lines and 2.0 for transformers, and it operates with a fixed 60-s time delay.

- **Underfrequency load shedding relays:** A three-stage load-shedding scheme is implemented using frequency relays. In the first stage, 20% of the connected load is shed when the system frequency drops below 58.5 Hz. The second stage sheds an additional 22.5% at 58.2 Hz, and the third stage disconnects a further 17.5% of the load if the frequency falls below 57.6 Hz.
- **Undervoltage and overvoltage protection of generators:** Generator voltage protection is provided by undervoltage and overvoltage relays set to operate at 0.9 p.u. and 1.1 p.u., respectively, with a time delay of 2 s to avoid unnecessary tripping during temporary voltage deviations.
- **Underfrequency and overfrequency protection of generators:** Generator frequency protection relays are configured with lower and upper frequency thresholds of 57.30 Hz and 61.68 Hz, respectively, to trip generators under severe frequency deviations. A very short time delay is introduced to approximate near-instantaneous tripping, which provides a more demanding condition for resilience assessment.

While this study is conducted on the IEEE 39-bus test system as a proof of concept, the proposed methodology is developed with scalability and practical applicability in mind. The protection models, VSC-HVDC control schemes, and DNS evaluation framework are implemented generically within PSS®E 34.9.6—an industry-standard simulation platform—which facilitates potential extension to larger networks without conceptual modification.

The computational burden increases with system size; however, given the focus of this work on offline planning and resilience assessment, the required simulations are performed periodically to support long-term decision-making rather than real-time operation. Moreover, the developed automation framework supports parallel execution, enabling large-scale contingency studies to be computationally manageable. Application to real transmission systems would require accurate system data, protection coordination settings, and validated dynamic models. Nevertheless, the underlying modeling and analysis framework is not restricted to the 39-bus system and can be adapted to practical networks. Consequently, the insights obtained—particularly regarding the resilience contributions of VSC-HVDC interconnections and the trade-offs in protection coordination—are relevant for real-world system planning and resilience enhancement studies.

6. Simulation Results

This section provides a comprehensive analysis of cascading failure simulations under higher-order contingency scenarios, specifically N-2 and N-3 events, which represent more severe and less probable disturbances than N-1 contingencies. In total, 300 randomly selected N-2 scenarios and 300 randomly selected N-3 scenarios involving line and transformer outages were examined. For each contingency type, half of the scenarios were assigned to the first subnetwork and the other half to the second subnetwork. The emphasis is not on the initiating events themselves, but rather on comparing the impacts of AC and DC interconnections in response to these disturbances. For each contingency category, key indices were computed based on the resulting DNS values, including total DNS, average DNS, and CVaR computed over the worst 10% of DNS outcomes. These aggregated metrics quantitatively assess system robustness and vulnerability under stressed operating conditions. Selecting 300 scenarios per contingency type represents a practical

trade-off between computational feasibility and scenario diversity, ensuring that the tail of worst-case outcomes is adequately represented for both interconnection configurations.

6.1. Results for N-2 Contingencies

Table 2 presents the results of the N-2 contingencies under two interconnection scenarios: one with an AC link and the other with a DC link.

Table 2. Aggregate DNS metrics for AC and DC interconnection configurations under N-2 contingency scenarios.

System		Statistical Parameters of DNS		
		Total (MW)	**Mean (MW)**	**CVaR (MW)**
With the AC link	IEEE 39 No. 1	493,037.53	1643.46	5304.48
	IEEE 39 No. 2	643,514.26	2145.05	6097.10
	Whole case study	1,135,151.49	3783.84	11,401.58
With the DC link	IEEE 39 No. 1	293,562.33	978.54	5304.48
	IEEE 39 No. 2	254,569.75	848.57	3486.68
	Whole case study	546,543.95	1821.81	6535.36

Table 2 shows that system resilience under N-2 contingency scenarios improves significantly when a DC link is employed. For example, the total DNS for the entire system decreases from 1,135,151.49 MW under the AC-link configuration to 546,543.95 MW under the DC-link configuration. This improvement is also evident in the analysis of each AC subnetwork individually. In the second subnetwork, for example, the average DNS decreases from 2145.05 MW to 848.57 MW, indicating a reduction of approximately 60.44%. Furthermore, the CVaR decreases from 11,401.58 MW to 6535.36 MW, corresponding to a 42.68% reduction. This notable decline in CVaR indicates that the DC interconnection not only reduces the average impact of contingencies but also significantly mitigates extreme failure cases, thereby limiting the risk of widespread cascading outages. One point that requires clarification in Table 2 is why the CVaR value for IEEE 39 No. 1 is identical under both AC and DC interconnection scenarios. This occurs because CVaR, computed at the 90% confidence level, represents the average of the worst 10% of DNS outcomes. In this study, with 300 simulation scenarios, this corresponds to the 30 worst-case outcomes. For IEEE 39 No. 1, these outcomes yield the same curtailed load of 5304.48 MW in both interconnection configurations. Therefore, despite differences in other statistical measures, such as the mean or total curtailed load, the CVaR remains unchanged, reflecting the system response's extreme-tail behavior rather than the overall distribution of DNS outcomes.

A detailed breakdown of DNS values for each subnetwork further demonstrates that the DC interconnection enhances overall system resilience.

Figures 6 and 7 present the frequency distribution of DNS values obtained from all simulated N-2 contingency events under AC and DC interconnection scenarios, respectively. The horizontal axis shows DNS value ranges (in MW), while the vertical axis indicates the number of events within each range.

The histograms in Figures 6 and 7 clearly show that the DC interconnection configuration results in fewer high-DNS events, indicating improved performance under N-2 contingencies. A comparison of the two figures further shows that the DC link yields a higher number of contingencies with no load shedding, namely 138 cases compared to 127 under the AC configuration, suggesting enhanced system stability under N-2 scenarios. In addition, the DC link significantly reduces the number of severe outcomes observed under the AC configuration. Specifically, under the AC setup, 45 contingencies lead to a

complete blackout of one subnetwork, while 51 contingencies result in the complete blackout of both subnetworks. In contrast, under the DC configuration, only 39 contingencies result in a complete blackout of one subnetwork. This indicates that the DC link effectively limits the extent of cascading failures and improves system resilience. In this study, a complete blackout is defined as the full disconnection of all loads in a subnetwork due to relay operations.

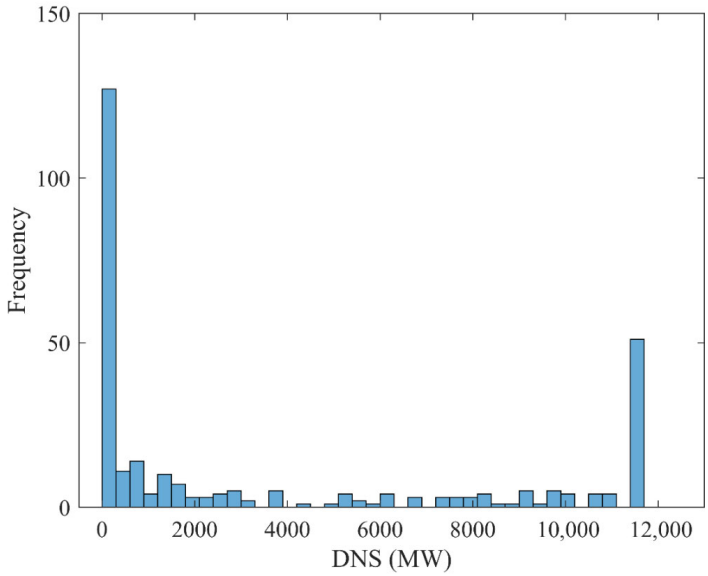

Figure 6. Frequency distribution of DNS under N-2 contingencies with AC interconnection.

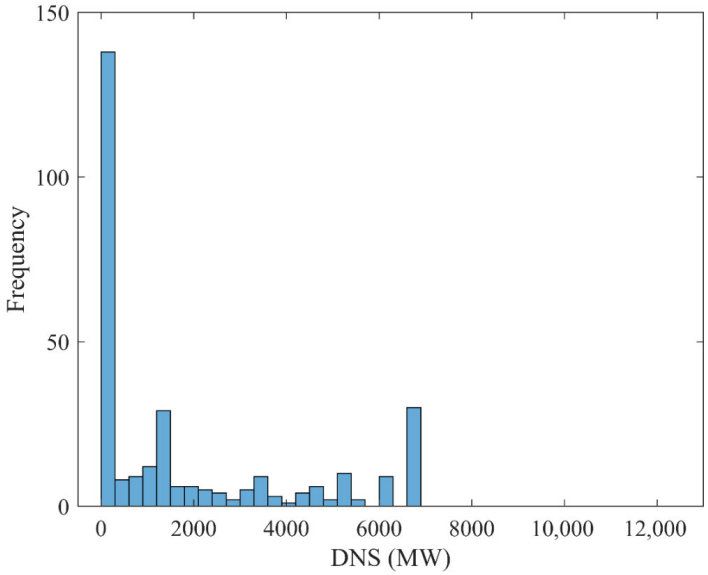

Figure 7. Frequency distribution of DNS under N-2 contingencies with DC interconnection.

To complement the comparison of the DNS distributions, statistical significance was assessed for the AC and DC cases using nonparametric tests on the DNS samples (Nc = 300 for each case). Distributional and paired differences across scenarios were evaluated using the two-sample Kolmogorov–Smirnov (KS) and Wilcoxon signed-rank tests, respectively. Tail risk was quantified by $CVaR_{0.9}$ defined as the mean of the worst 10% of DNS outcomes, and uncertainty was characterized via bootstrap 95% confidence intervals (CIs) using B = 5000 resamples. Table 3 summarizes the results, including the KS and Wilcoxon p-values, $CVaR_{0.9}$ estimates, and bootstrap CIs for both configurations.

Table 3. Statistical comparison of DNS between AC and DC interconnections for N-2 contingencies.

Metric	AC Link	DC Link	Difference (AC-DC)
$CVaR_{0.9}$ (MW)	11,401.58	6535.36	4866.22
95% CIs for $CVaR_{0.9}$ (MW)	[11,401.58, 11,401.58]	[6243.72, 6630.98]	[4770.59, 5157.85]
KS statistic, D	-	-	0.3033
KS test p-value	-	-	1.15×10^{-12}
Wilcoxon signed-rank statistic	-	-	4.7130
Wilcoxon signed-rank p-value	-	-	2.44×10^{-16}
Bootstrap p-value for $\Delta CVaR$	-	-	$p < 2 \times 10^{-4}$

Table 3 summarizes the statistical evidence for comparing DNS outcomes between the AC and DC cases across the 300 simulated scenarios. The two-sample KS test evaluates whether the empirical distributions differ significantly, while the Wilcoxon signed-rank test assesses whether the paired scenario-wise differences between the two cases are statistically significant. In addition, $CVaR_{0.9}$ is reported to characterize tail risk, i.e., the average DNS over the worst 10% of outcomes, together with bootstrap 95% CIs. Overall, the table provides a rigorous complement to the graphical distribution comparison, showing that the observed AC–DC differences are unlikely to be attributable to sampling variability and quantifying the magnitude and uncertainty of the tail-risk reduction.

To further investigate system behavior, the total load profile for the case study was analyzed under a representative N-2 contingency scenario involving the outages of lines 10–11 and 26–28 in the first subnetwork. Figure 8 illustrates the resulting load dynamics for the AC and DC interconnection configurations.

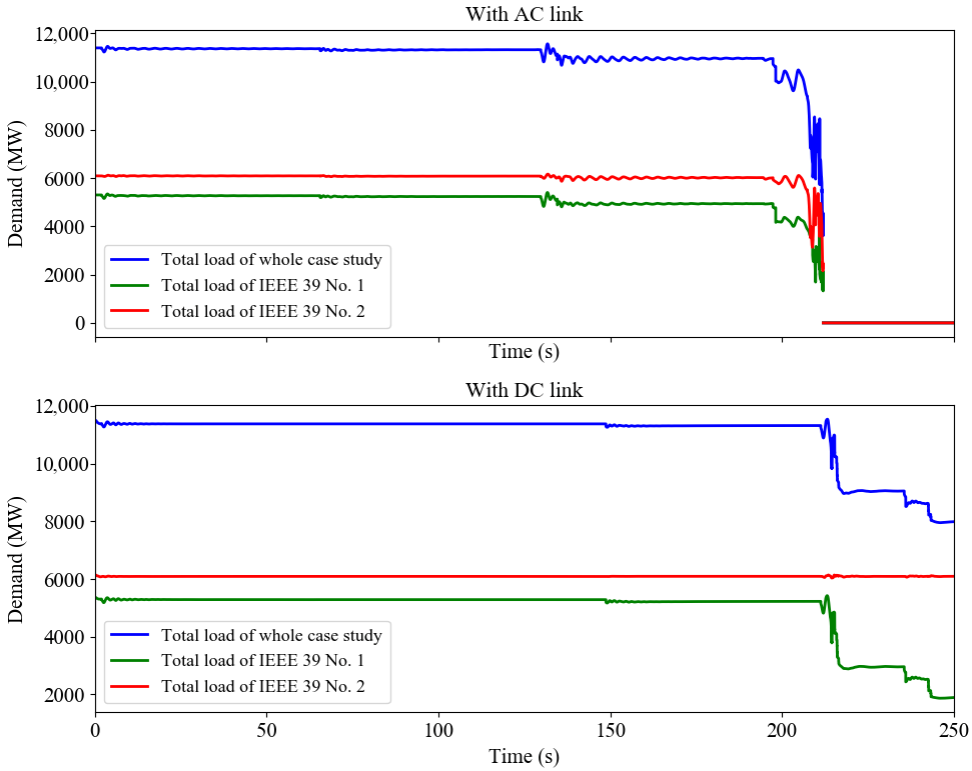

Figure 8. System load dynamics under a representative N-2 contingency scenario involving the outage of lines 10–11 and 26–28 in IEEE 39 No. 1, comparing the AC and DC interconnection configurations.

As illustrated in Figure 8, disturbances begin to intensify around 200 s in the AC interconnection case, leading to progressive load shedding. By 211 s, cascading failures result in a complete blackout in both subnetworks. In contrast, with the DC interconnection, subnetwork 2 remains fully operational throughout the event, while subnetwork 1 experiences partial load shedding at 217, 236, and 243 s. These findings indicate that the DC link enhances disturbance isolation and system stability under severe contingencies.

To further examine the dynamic response of the VSC-HVDC link, Figure 9 presents the AC- and DC-side currents in response to this contingency. Both currents initially respond to the disturbance and then gradually stabilize, reaching nearly constant values within 20-30 s. This behavior highlights the HVDC link's ability to sustain power transfer between the subnetworks and mitigate fluctuations under severe AC-side contingencies.

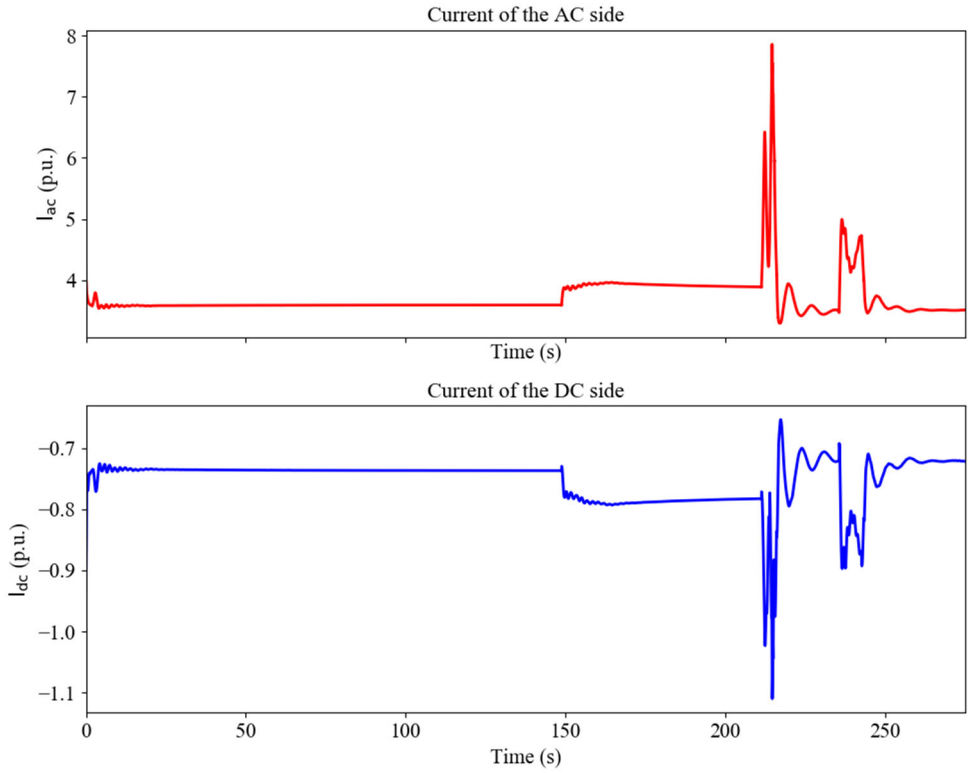

Figure 9. Dynamics of the AC- and DC-side currents of the VSC-HVDC link under a representative N-2 contingency scenario involving the outage of lines 10–11 and 26–28 in IEEE 39 No. 1, showing oscillatory behavior followed by gradual damping and stabilization.

6.2. Results for N-3 Contingencies

The results of the N-3 contingency scenarios are summarized in Table 4. The accompanying histograms showing the distribution of DNS values under AC and DC configurations are displayed in Figures 10 and 11, respectively.

The results obtained for the N-3 contingency scenarios include the following key points:

- The total DNS decreases from 1,452,636.88 MW under the AC link to 737,668.40 MW with the DC link, corresponding to an improvement of approximately 49.22%.
- The CVaR of DNS is reduced from 11,401.58 MW (AC) to 6629.73 MW (DC), reflecting a decrease of approximately 41.85%.
- The average DNS of the first subnetwork under the DC link is reduced by about 37.65% compared with the AC link case.
- The number of contingencies requiring no load shedding increases from 74 (AC) to 85 (DC), indicating enhanced system resilience.

- The number of contingencies causing a complete blackout of one subnetwork decreases significantly from 46 (AC) to 37 (DC).
- The number of contingencies resulting in a total blackout of both subnetworks is reduced from 70 under AC to zero when the DC link is in place.

Table 4. Aggregate DNS metrics for AC and DC interconnection configurations under N-3 contingency scenarios.

System		Statistical Parameters of DNS		
		Total (MW)	**Mean (MW)**	**CVaR (MW)**
With the AC link	IEEE 39 No. 1	652,945.32	2176.48	5304.48
	IEEE 39 No. 2	801,206.46	2670.69	6097.10
	Whole case study	1,452,636.88	4842.12	11,401.58
With the DC link	IEEE 39 No. 1	407,137.52	1357.13	5304.48
	IEEE 39 No. 2	332,168.51	1107.23	4038.84
	Whole case study	737,668.40	2458.89	6629.60

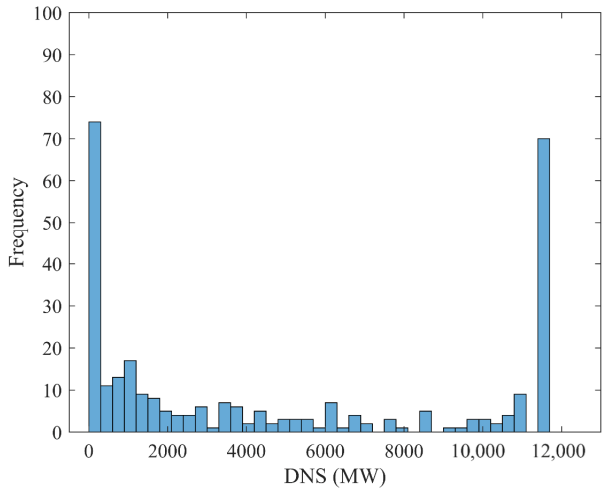

Figure 10. Frequency distribution of DNS under N-3 contingencies with AC interconnection.

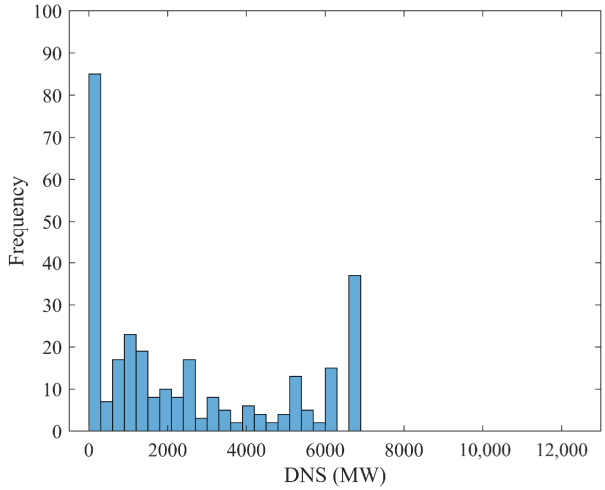

Figure 11. Frequency distribution of DNS under N-3 contingencies with DC interconnection.

Table 5 reports the results of the nonparametric significance tests and tail-risk metrics ($CVaR_{0.9}$ with bootstrap 95% CIs) derived from DNS for the AC and DC interconnection configurations under N-3 contingencies, based on 300 paired simulated scenarios.

Table 5. Statistical comparison of DNS between AC and DC interconnections for N-3 contingencies.

Metric	AC Link	DC Link	Difference (AC-DC)
$CVaR_{0.9}$ (MW)	11,401.58	6629.73	4771.85
95% CIs for $CVaR_{0.9}$ (MW)	[11,401.58, 11,401.58]	[6484.05, 6634.92]	[4766.66, 4917.53]
KS statistic, D	-	-	0.3467
KS test p-value	-	-	2.05×10^{-16}
Wilcoxon signed-rank statistic	-	-	5.1539
Wilcoxon signed-rank p-value	-	-	2.55×10^{-7}
Bootstrap p-value for $\Delta CVaR$	-	-	$p < 2 \times 10^{-4}$

Table 5 complements the empirical frequency plots by providing quantitative statistical evidence that the AC–DC differences in DNS are unlikely to be due to sampling variability. In particular, the KS and Wilcoxon signed-rank test results confirm statistically significant differences between the two cases, while the $CVaR_{0.9}$ estimates and their bootstrap 95% CIs quantify the magnitude and uncertainty of the tail-risk reduction achieved with the DC interconnection.

In summary, the comprehensive dynamic simulations conducted across the N-2 and N-3 contingency scenarios demonstrate a clear advantage of using a DC interconnection over an AC link. The DC configuration consistently leads to significant reductions in total DNS, average DNS, and CVaR while also reducing the frequency and severity of network blackouts. In addition, combining dynamic simulations with the DNS index enables a more accurate and realistic assessment of system vulnerability by capturing time-dependent cascading failures and the operation of protective devices, which are often overlooked in static analyses. These results highlight the important role of DC links in enhancing the robustness and resilience of interconnected power systems.

6.3. DNS Sensitivity to Overcurrent Relay Settings

To further assess the impact of protective relay settings on system performance, an additional scenario was analyzed in which the THR factor of the overload detection relays on transmission lines was increased from 1.05 to 1.1. This adjustment was used to evaluate the effect of a delayed protection response on DNS levels, blackout severity, and overall system resilience during cascading failure conditions.

The selected range of 1.05–1.1 p.u. reflects practically relevant overload protection settings in transmission system operation. While 1.05 p.u. represents a conventional overload alarm threshold, 1.1 p.u. is consistent with commonly adopted short-term emergency thermal ratings of overhead conductors under typical operating conditions. Higher values would exceed realistic thermal margins for sustained operation and could lead to unacceptable thermal stress and long-term mechanical degradation of conductors. Therefore, the considered range captures the transition from standard protection sensitivity to delayed relay operation near emergency thermal limits.

Box plots were generated to depict the distribution of DNS values across all N-3 contingency scenarios for THR = 1.05 and THR = 1.1, thereby evaluating the influence of adjusted overload protection thresholds on system resilience. Figures 12 and 13 present these distributions for the AC and DC interconnection configurations, respectively. These

visualizations highlight the impact of relay sensitivity on load curtailment by showing changes in the median, interquartile range, and overall variability of DNS values. Notably, the DC interconnection consistently exhibits lower median DNS and reduced dispersion under both settings, underscoring its superior ability to maintain system stability even with delayed overload detection.

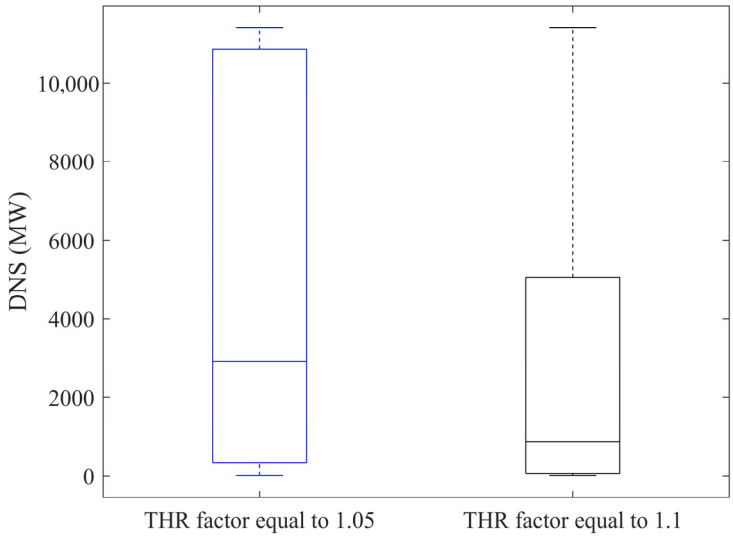

Figure 12. Box plots of DNS values under N-3 contingencies for AC interconnection with two overload thresholds.

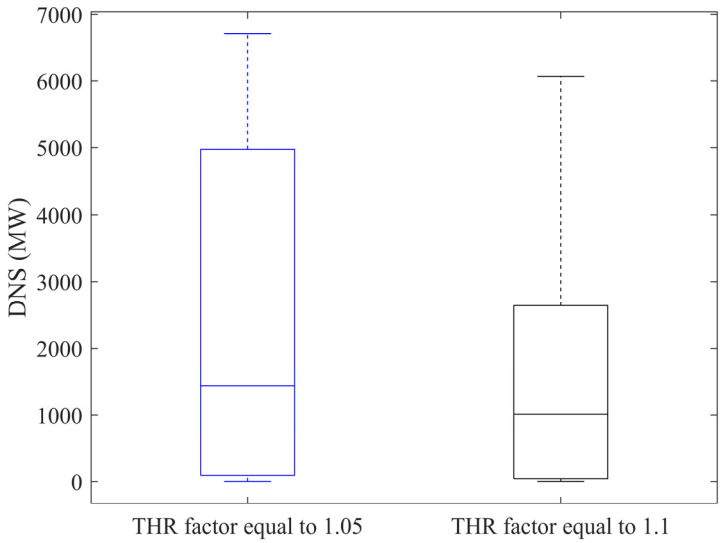

Figure 13. Box plots of DNS values under N-3 contingencies for DC interconnection with two overload thresholds.

The results indicate that increasing the overload protection threshold from 1.05 to 1.1 significantly reduces total DNS in the AC interconnection, from 1,452,636.88 MW to 962,928.14 MW (a 33.7% decrease), highlighting the strong influence of protection sensitivity on cascading-failure propagation. Similarly, under the DC interconnection configuration, the same adjustment leads to a 33.1% reduction, from 737,668.40 MW to 493,303.70 MW. Importantly, the DC-linked system consistently outperforms its AC counterpart, maintaining lower DNS levels across both threshold settings.

From a protection engineering perspective, these results highlight an inherent trade-off between relay sensitivity and system-level resilience. Lower overload thresholds (e.g.,

THR = 1.05) ensure faster isolation of overloaded elements and enhanced equipment protection but may unintentionally accelerate cascading disconnections by removing lines before power flows can naturally redistribute. Conversely, slightly higher thresholds (THR = 1.1) allow temporary overload tolerance, providing the system with additional time to rebalance flows and potentially contain cascading propagation. However, this delayed intervention increases thermal stress on conductors and may increase the risk of long-term mechanical degradation or insulation deterioration. Therefore, optimal relay coordination should not be determined solely based on local equipment protection criteria but must also consider system-wide resilience objectives under high-impact contingencies.

These findings further confirm the superior capability of DC interconnections to limit disturbance propagation and contain cascading failures, even under less conservative overload-protection settings. While this study examines the sensitivity of cascading failures to overload relay thresholds, future work could extend the analysis to a broader range of protection strategies, including distance protection coordination, adaptive protection schemes, and their interactions with VSC-HVDC controls.

7. Conclusions

This paper presents a dynamic resilience assessment of hybrid AC/DC power systems across a range of outage contingency scenarios. Time-domain simulations were conducted in PSS®E 34.9.6 to evaluate system performance under N-2 and N-3 events, with a focus on comparing AC and DC interconnection configurations. Unlike previous studies, this work provides a quantitative evaluation of resilience using the DNS index derived from dynamic time-domain simulations. It further examines the role of DC interconnections in mitigating cascading failures and highlights the influence of protection thresholds on system resilience. Collectively, these contributions offer new insights into the design and operation of resilient hybrid networks.

The results demonstrate that the DC interconnection not only reduces total and average DNS values but also significantly lowers the severity of extreme events, as indicated by reduced CVaR values. Furthermore, the DC link improves system performance by limiting the propagation of disturbances and reducing the risk of widespread outages. In addition, the study examined the impact of varying overload protection thresholds by adjusting the relay trip settings from 1.05 to 1.1. The results show that increasing the threshold reduces total DNS in both AC and DC configurations. However, the DC-linked system consistently demonstrates superior performance, exhibiting lower DNS levels and better disturbance isolation.

Importantly, this study highlights the value of dynamic simulation approaches over traditional static analyses. By capturing the behavior of protection systems and system responses to outages, dynamic simulations offer a more accurate and operationally meaningful understanding of system resilience, particularly under high-impact, low-probability events. These findings support the integration of VSC-HVDC technology as a practical solution for improving system-wide resilience in future grid development. It is noteworthy that analyzing DC-side faults in the present study is not straightforward and will be considered a topic for future research.

Author Contributions: Conceptualization, S.R.-M., L.S. and A.G.-C.; methodology, L.S.; software, S.R.-M. and L.S.; validation, S.R.-M., L.S. and A.G.-C.; formal analysis, L.S.; investigation, S.R.-M. and L.S.; resources, S.R.-M.; data curation, S.R.-M. and L.S.; writing—original draft preparation, S.R.-M.; writing—review and editing, L.S. and A.G.-C.; visualization, S.R.-M.; supervision, L.S. and A.G.-C.; project administration, L.S. and A.G.-C.; funding acquisition, L.S. and A.G.-C. All authors have read and agreed to the published version of the manuscript.

Funding: HVDC-WISE is supported by the European Union's Horizon Europe program under agreement 101075424. UK Research and Innovation (UKRI) funding for HVDC-WISE is provided under the UK government's Horizon Europe funding guarantee [grant numbers 10041877 and 10051113].

Data Availability Statement: Due to privacy and confidentiality agreements related to engineering design, detailed data supporting the results reported in this article, including schematics and related technical documents, cannot be made publicly available. Further inquiries can be directed to the corresponding author.

Conflicts of Interest: The authors have no affiliations or involvement with any organization or entity that has any financial interest (such as honoraria, educational grants, participation in speakers' bureaus, membership, employment, consultancies, stock ownership or other equity interests, expert testimony, or patent-licensing arrangements) or non-financial interest (such as personal or professional relationships, affiliations, knowledge, or beliefs) related to the content of this manuscript. The authors confirm that this work is purely academic and research-oriented.

References

1. Sun, K. (Ed.) *Cascading Failures in Power Grids*; Springer International Publishing: Cham, Switzerland, 2024. [CrossRef]
2. Hashemi, S.; Panteli, M.; Baù, M.; Ciapessoni, E.; Cirio, D.; Pitto, A.; Bakhos, G.; Barla, N.; Benchaib, A.; Ismail, B.; et al. Tools for Reliability and Resilience-Oriented Planning and Operation of Hybrid AC/DC Power Systems. In Proceedings of the 2024 IEEE PES Innovative Smart Grid Technologies Europe (ISGT EUROPE), Istanbul, Turkey, 21–24 October 2024; pp. 1–5. [CrossRef]
3. Dehghanian, P.; Aslan, S.; Dehghanian, P. Maintaining Electric System Safety through an Enhanced Network Resilience. *IEEE Trans. Ind. Appl.* **2018**, *54*, 4927–4937. [CrossRef]
4. Hussan, U.; Hassan, M.; Ayub, M.A.; Peng, J.; Rasheed, H.; Jiang, H.; Asghar, F. Smooth and uninterrupted operation of standalone DC microgrid under high and low penetration of RESs. *IEEE Access* **2024**, *12*, 48620–48629. [CrossRef]
5. Mohammadi, F.; Rouzbehi, K.; Hajian, M.; Niayesh, K.; Gharehpetian, G.B.; Saad, H.; Sood, V.K. HVDC Circuit Breakers: A Comprehensive Review. *IEEE Trans. Power Electron.* **2021**, *36*, 13726–13739. [CrossRef]
6. Adewolu, B.O.; Saha, A.K. Contingency Control Capability of an Optimized HVDC-Based VSC Transmission System. *IEEE Access* **2020**, *9*, 4112–4128. [CrossRef]
7. Strunz, K.; Schilling, S.; Kuschke, M.; Czerwinska, A. Fast Contingency Analysis and Control for Overload Mitigation in Integrated High Voltage AC and Multi-Terminal HVDC Grids. *IEEE Trans. Power Syst.* **2023**, *39*, 5575–5590. [CrossRef]
8. Meyer-Huebner, N.; Weck, S.; Bennewitz, F.; Suriyah, M.; Bhalodi, K.; Giuntoli, M.; Biagini, V.; Krontiris, A.; Wasserrab, A.; Ndreko, M.; et al. N-1-Secure Dispatch Strategies of Embedded HVDC Using Optimal Power Flow. In Proceedings of the 2018 IEEE Power & Energy Society General Meeting (PESGM), Portland, OR, USA, 5–9 August 2018; pp. 1–5. [CrossRef]
9. Castro, L.M.; Acha, E.; Rodriguez-Rodriguez, J.R. Efficient Method for the Real-Time Contingency Analysis of Meshed HVDC Power Grids Fed by VSC Stations. *IET Gener. Transm. Distrib.* **2018**, *12*, 3158–3166. [CrossRef]
10. Sass, F.; Rothstein, A.; Staudt, V.; Westermann, D. Critical Contingency Management Based on Characteristic Fault Pattern for AC-HVDC Systems. In Proceedings of the 13th IET International Conference on AC and DC Power Transmission (ACDC 2017), Stevenage, UK, 28 February–2 March 2017; p. 42. [CrossRef]
11. Vitulano, L.C.; L'Abbate, A.; Calisti, R.; Sessa, S.D. Analyses of Contingencies Impact and Key Benefits in a HVAC-to-HVDC OHL Conversion Study Case. In Proceedings of the 2023 AEIT International Annual Conference (AEIT), Turin, Italy, 18–20 October 2023; pp. 1–6. [CrossRef]
12. Dong, X.; Guan, E.; Jing, L.; Wang, H.; Mirsaeidi, S. Simulation and Analysis of Cascading Faults in Hybrid AC/DC Power Grids. *Int. J. Electr. Power Energy Syst.* **2020**, *115*, 105492. [CrossRef]
13. Hashemi, S.; Asprou, M.; Hadjidemetriou, L.; Panteli, M. Quantifying and mitigating cascading impacts in HVdc-interconnected power grids. *IEEE Access* **2025**, *13*, 154491–154507. [CrossRef]
14. Leelaruji, R.; Vanfretti, L.; Ghandhari, M.; Söder, L. Coordination of Protection and VSC-HVDC Systems for Mitigating Cascading Failures. In Proceedings of the 2010 International Conference on Power System Technology (POWERCON 2010), Zhejiang, China, 24–28 October 2010. [CrossRef]
15. Mirsaeidi, S.; Dong, X. An Integrated Control and Protection Scheme to Inhibit Blackouts Caused by Cascading Fault in Large-Scale Hybrid AC/DC Power Grids. *IEEE Trans. Power Electron.* **2019**, *34*, 7278–7291. [CrossRef]
16. Wang, B.; Camacho, J.A.; Pulliam, G.M.; Etemadi, A.H.; Dehghanian, P. New Reward and Penalty Scheme for Electric Distribution Utilities Employing Load-Based Reliability Indices. *IET Gener. Transm. Distrib.* **2018**, *12*, 3647–3654. [CrossRef]

17. Wang, J.; Wang, W.Q.; Wang, H.Y. Bi-Stage Operation Optimization of Active Distribution Networks with Soft Open Point Considering Violation Risk. *Energy Rep.* **2022**, *8*, 14947–14961. [CrossRef]
18. Renedo, J.; García-Cerrada, A.; Rouco, L. Active power control strategies for transient stability enhancement of AC/DC grids with VSC-HVDC multi-terminal systems. *IEEE Trans. Power Syst.* **2016**, *31*, 4595–4604. [CrossRef]
19. Beerten, J.; Gomis-Bellmunt, O.; Guillaud, X.; Rimez, J.; van der Meer, A.; Van Hertem, D. Modeling and Control of HVDC Grids: A Key Challenge for the Future Power System. In Proceedings of the Power Systems Computation Conference (PSCC 2014), Wrocław, Poland, 16–20 June 2014. [CrossRef]
20. Prieto Rodríguez de Vera, C. Development of a PSS/E Tool for Simulating Multiple High Voltage Direct Current Multiterminal Links with Voltage Source Converters. Master's Thesis, Department of Electrical Engineering, Comillas Pontifical University, Madrid, Spain, 2023.
21. D Chainho, P.J. General Modeling of Multi-Terminal VSC-HVDC Systems for Transient Stability Analysis. Master's Thesis, Universidade Técnica de Lisboa, Lisbon, Portugal, 2012.
22. Beerten, J.; Cole, S.; Belmans, R. Modeling of Multi-Terminal VSC HVDC Systems with Distributed DC Voltage Control. *IEEE Trans. Power Syst.* **2014**, *29*, 34–42. [CrossRef]
23. Cole, S.; Beerten, J.; Belmans, R. Generalized Dynamic VSC MTDC Model for Power System Stability Studies. *IEEE Trans. Power Syst.* **2010**, *25*, 1655–1662. [CrossRef]
24. Daelemans, G.; Srivastava, K.; Reza, M.; Cole, S.; Belmans, R. Minimization of Steady-State Losses in Meshed Networks Using VSC HVDC. In Proceedings of the IEEE/PES General Meeting, Calgary, AB, Canada, 26–30 July 2009; pp. 1–5. [CrossRef]
25. Renedo, J.; Sigrist, L.; Rouco, L.; Garcia-Cerrada, A. Impact on Power System Transient Stability of AC-Line-Emulation Controllers of VSC-HVDC Links. In Proceedings of the 2021 IEEE Madrid PowerTech, Madrid, Spain, 28 June–2 July 2021; pp. 1–6. [CrossRef]
26. Rodríguez-Pérez, N.; Matanza, J.; Sigrist, L.; Rueda Torres, J.; López, G. MaDIoT 3.0: Assessment of attacks to distributed energy resources and demand in a power system. *IEEE Open Access J. Power Energy* **2025**, *12*, 552–563. [CrossRef]
27. Rafinia, A.; Rezaei, N.; Moshtagh, J. Optimal Design of an Adaptive Under-Frequency Load Shedding Scheme in Smart Grids Considering Operational Uncertainties. *Int. J. Electr. Power Energy Syst.* **2020**, *121*, 106137. [CrossRef]
28. Asoh, D.A.; Chia, L.N. Design and Implementation of an Automatic Over/Undervoltage Protection System for Single-Phase Low Voltage Power Lines. *J. Power Energy Eng.* **2022**, *10*, 12–25. [CrossRef]
29. Samaan, N.A.; Dagle, J.E.; Makarov, Y.V.; Diao, R.; Vallem, M.R.; Nguyen, T.B.; Miller, L.; Vyakaranam, B.; Tuffner, F.; Pai, M.; et al. Modeling of Protection in Dynamic Simulation Using Generic Relay Models and Settings. In Proceedings of the 2016 IEEE Power and Energy Society General Meeting (PESGM), Boston, MA, USA, 17–21 July 2016; pp. 1–5. [CrossRef]
30. IEEE 39-Bus System. Available online: https://icseg.iti.illinois.edu/ieee-39-bus-system/ (accessed on 9 March 2026).
31. Athay, T.; Podmore, R.; Virmani, S. A Practical Method for the Direct Analysis of Transient Stability. *IEEE Trans. Power App. Syst.* **2007**, *PAS-2*, 573–584. [CrossRef]